

Maximum Likelihood Estimation of Log-Concave Densities on Tree Space

Yuki Takazawa

Department of Mathematical Informatics,
Graduate School of Information Science and Technology,
University of Tokyo

and

Tomonari Sei

Department of Mathematical Informatics,
Graduate School of Information Science and Technology,
University of Tokyo

November 23, 2022

Abstract

Phylogenetic trees are key data objects in biology, and the method of phylogenetic reconstruction has been highly developed. The space of phylogenetic trees is a nonpositively curved metric space. Recently, statistical methods to analyze the set of trees on this space are being developed utilizing this property. Meanwhile, in Euclidean space, the log-concave maximum likelihood method has emerged as a new nonparametric method for probability density estimation. In this paper, we derive a sufficient condition for the existence and uniqueness of the log-concave maximum likelihood estimator on tree space. We also propose an estimation algorithm for one and two dimensions.

Since various factors affect the inferred trees, it is difficult to specify the distribution of sample trees. The class of log-concave densities is nonparametric, and yet the estimation can be conducted by the maximum likelihood method without selecting hyperparameters. We compare the estimation performance with a previously developed kernel density estimator numerically. In our examples where the true density is log-concave, we demonstrate that our estimator has a smaller integrated squared error when the sample size is large. We also conduct numerical experiments of clustering using the Expectation-Maximization (EM) algorithm and compare the results with k-means++ clustering using Fréchet mean.

Keywords: nonparametric density estimation; phylogenetic tree; clustering; CAT(0) space

1 Introduction

Inference of phylogeny is one of the key problems in biology. Phylogenetic trees represent the evolutionary histories of taxa. The methods of phylogenetic reconstruction using current gene data have been highly developed, and it is now possible to reconstruct them easily with various models and inference methods (Felsenstein, 2004).

However, due to the uncertainty of inference, incomplete lineage sorting or irregular biological processes such as horizontal transfer, it is usually the case that different gene loci indicate different evolutionary histories (Reid et al., 2014). The classical approach to this problem is finding a *consensus tree* (Bryant, 2003), a single summary tree of multiple trees inferred from different loci, which is constructed by some rules. In 2001, Billera et al. (2001) introduced the space of phylogenetic trees with n leaves, *tree space*, which is a geodesic metric space with nonpositive curvature. Recent research has shifted to the statistical analysis of a set of trees in such spaces, enabling a geometrical perspective. These efforts include point estimation by Fréchet mean (Benner et al., 2014), principal component analysis (Nye, 2011), outlier detection using a kernel density estimator (Weyenberg et al., 2014, 2017), and construction of confidence sets (Willis, 2019).

Since numerous factors affect the inferred phylogenetic trees, the parametric approach to specifying the distribution of inferred trees is difficult, and the risk of misspecifying models is high. In this sense, the nonparametric approach generally specifies fewer constraints in the distribution and might be desirable. The kernel density estimator proposed in Weyenberg et al. (2014, 2017) is designed for this purpose.

In Euclidean space, log-concave density estimation has emerged as a new shape-constrained, nonparametric method of density estimation. Log-concave density is a class of probability densities whose logarithm are concave functions. Compared to classical smoothing approaches such as kernel density estimates, in which we need to specify some hyperparameters such as bandwidths, log-concave density has an advantageous property that the estimation can be done automatically. Concretely, it has been shown that the maximum likelihood estimators exist in both the one-dimensional and multi-dimensional cases and that the calculation of the estimators can be reduced to a convex optimization problem in \mathbb{R}^n with n sample points (Cule et al., 2010).

In this paper, we show that the maximum likelihood estimator of log-concave density in tree space exists under some conditions and that the estimation can be implemented in the one-dimensional case. Although we do not derive an algorithm for multidimensional cases due to the difficulty of finding the closure of convex hulls, we also show that we can approximately calculate the maximum likelihood estimator in the two-dimensional case.

The remaining sections are organized as follows. In section 2, we review some basic concepts of tree space and define some concepts for convex analysis in Hadamard spaces. Section 3 presents our main result for maximum likelihood estimation in tree space, in one dimension and multiple dimensions. Section 4 explains how to calculate the maximum likelihood estimator in the one-dimensional and two-dimensional cases. Section 5 shows the results of simulation studies. We compare the performance of density estimation with the kernel density estimator. We also compare the simulation results of clustering with a mixture of log-concave densities to the k-means++ approach using the Fréchet mean.

2 Preliminaries

2.1 Phylogenetic Trees and Tree Space

A phylogenetic tree is modeled as a tree with labels only on the leaves. We call a tree with $n + 1$ labeled leaves an n -tree. n -trees have one root leaf representing the common ancestor and n leaves representing present taxa. Internal edges are edges that are not directly connected to leaves. In binary n -trees, it is easy to see that the number of internal edges is $n - 2$. Nonbinary trees have fewer internal edges since they can be obtained by contracting some internal edges of some binary trees. The number of different topologies for binary n -trees is $(2n - 3)!!$ (Felsenstein, 1978). Note that the edges in different tree topologies can be regarded as the same if they partition the leaves in the same way. If each internal edge in an n -tree has a positive length, we call it a *metric n -tree*.

Billera et al. (2001) modeled the space of metric n -trees as follows. First, each binary tree topology is modeled as a positive Euclidean orthant with dimension $n - 2$, with each axis corresponding to the length of each internal edge of that topology. These orthants are stuck together on the axes representing the same edges. Nonbinary trees constitute the

boundaries of these orthants since they are obtained by contracting some internal edges. In particular, the n -tree without any internal edges is the point located at the center of tree space connected to every orthant. We call this point the *origin* in this paper. The space of metric n -trees obtained in this way is called *tree space* and is denoted as \mathcal{T}_n .

In this paper, we mainly discuss the results in the one-dimensional or two-dimensional case. By dimension, we mean the dimension of each orthant or the dimension of the space seen as a cubical complex. Therefore, by the p -dimensional tree space, we mean the space \mathcal{T}_{p+2} . In the one-dimensional tree space, we only have $3!! = 3$ topologies and each orthant representing some topology is a half-line connected to the other two at the origin, the point representing a trifurcating tree (Figure 1). Two-dimensional tree space \mathcal{T}_4 has $5!! = 15$ topologies, each orthant being a nonnegative Euclidean plane, and three different orthants are connected to each axis (Figure 1). It is known that if we represent each axis as a vertex and each orthant as an edge connecting two vertices, then the whole of space \mathcal{T}_4 can be graphically depicted as a Petersen graph, as shown in Figure 1. For details, see Billera et al. (2001) or Lubiw et al. (2020), for example.

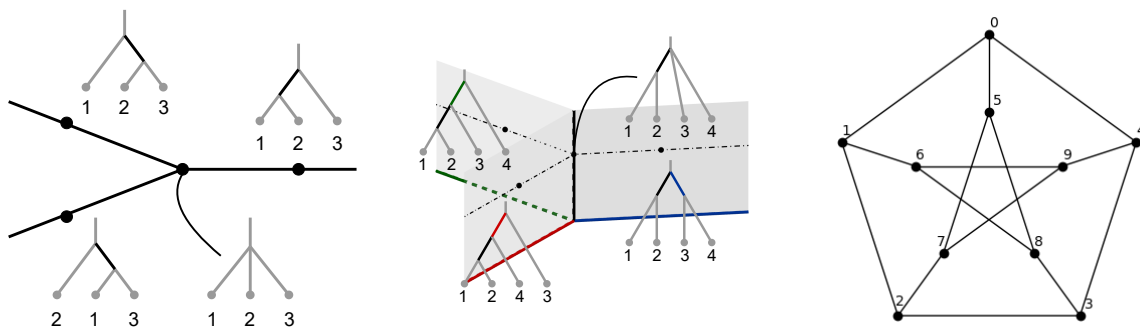


Figure 1: Depiction of tree space. (Left): one-dimensional tree space \mathcal{T}_3 , consisting of three half-lines each corresponding to a topology. (Center): part of two-dimensional tree space. (Right): Petersen graph. Each edge represents a 2-dimensional orthant in \mathcal{T}_4 with endpoints representing axes constituting the boundaries. Vertices corresponding to axes are indexed from 0 to 9 for convenience.

2.2 Geometry of Tree Space

Tree space can be readily formulated as a metric space. Since it is the union of Euclidean orthants, we can simply define the distance between two points in the same orthant as the usual Euclidean distance. For any two points in distinct orthants, we can set the distance between them as the infimum of the lengths of paths with endpoints in those two points. The infimum is attained since tree space consists of a finite number of orthants, and once a sequence of orthants of a path is decided, there is a unique path with minimum length. The paths which attain the minimum distances are called *geodesics*, and a metric space with a geodesic between any two points is called a *geodesic metric space*.

Tree space is also known to be a *Hadamard* space; i.e., it is a complete metric space with nonpositive curvature. See, for example, Bačák (2014) for proof. This property is key to many important results in this space. In Hadamard spaces, the geodesic connecting any two points is guaranteed to be unique. Owen and Provan (2011) has developed an algorithm to find geodesics in tree space in $O(p^4)$ time, where p denotes the dimension of tree space. In tree space, geodesics are piecewise segments through sequences of orthants, and in some cases, they become *cone paths*, where each geodesic consists of two segments connecting the endpoints and the origin. In particular, in two-dimensional tree space \mathcal{T}_4 , whether a geodesic between two points becomes a cone path depends only on the “angle” between them. See, for example, Lubiw et al. (2020) for a detailed account of this property. The nonpositively curved property also results in the existence and uniqueness of the *Fréchet mean*. The Fréchet mean μ of given samples $X_1, \dots, X_n \in \mathcal{H}$ and weights w_1, \dots, w_n is defined as the minimizer of the sum of squared distance:

$$\mu = \arg \min_{x \in \mathcal{H}} \sum_{i=1}^n w_i d(x, X_i)^2. \quad (1)$$

It is a generalization of the arithmetic mean since they coincide with uniform weights in Hilbert spaces. It is known that the Fréchet mean can be calculated using the proximal point algorithm (Bačák, 2013). See, for example, Bačák (2014) for proof of results regarding the Fréchet mean in Hadamard spaces.

2.3 Convex Sets and Concave Functions on Hadamard Spaces

In this section, we define several concepts of convex sets and concave functions on Hadamard spaces.

First, we define convex sets as in Bačák (2014). Let (\mathcal{H}, d) be a Hadamard space and for any points $x, y \in \mathcal{H}$, let $[x, y]$ denote the unique geodesic between them. Also, for $\lambda \in [0, 1]$, we use informally the notation $(1 - \lambda)x + \lambda y$ to denote the points in the geodesic $[x, y]$ with distance $\lambda d(x, y)$ from x . We say $A \subseteq \mathcal{H}$ is convex if for any points $x, y \in A$ we have $[x, y] \subseteq A$.

Function $f : \mathcal{H} \rightarrow [-\infty, \infty]$ is concave if its hypograph $\text{hyp}f = \{(x, \mu) \in \mathcal{H} \times \mathbb{R} \mid \mu \leq f(x)\}$ is convex. Note that a product of Hadamard spaces is also a Hadamard space, and thus, in particular, $\mathcal{H} \times \mathbb{R}$ is also a Hadamard space. An equivalent definition of concavity of a function f can be given in the following way: given any points $x, y \in \mathcal{H}$, if $\alpha < f(x)$ and $\beta < f(y)$, then for any $\lambda \in (0, 1)$, $f((1 - \lambda)x + \lambda y) > (1 - \lambda)\alpha + \lambda\beta$.

Given any set S in \mathcal{H} , a convex hull of S is the smallest convex set in \mathcal{H} containing S . This set exists because the intersection of (possibly infinite) convex sets is convex and that \mathcal{H} is convex. We denote the convex hull of S as $\text{conv } S$. In Hadamard spaces, it is known that a convex hull can be written as in the following Lemma.

Lemma 1 (Bačák (2014), Lemma 2.1.8). *For $S \subseteq \mathcal{H}$, put $C_0 = S$ and for $n \in \mathbb{N}$, recursively define C_n by*

$C_n = \{x \in \mathcal{H} \mid x \text{ is in a geodesic between points in } C_{n-1}\}$. Then,

$$\text{conv } S = \bigcup_{n=0}^{\infty} C_n. \quad (2)$$

This Lemma indicates that taking geodesics between points an infinite number of times obtains the convex hull. Next, we define an important concept of the concave hull of a function. Given any function f on \mathcal{H} , the concave hull of f , $\text{conc } f$, is defined as the least concave function minorized by f . Its existence and uniqueness in Euclidean space is a well-known result; see chapter 5 of Rockafellar (1970) for a detailed account. Here we show the existence and uniqueness of the Hadamard case, but as we will see, the proof proceeds in the same way as in the Euclidean case.

Lemma 2. *For any function $f : \mathcal{H} \rightarrow [-\infty, \infty]$, the concave hull $\text{conc } f$ exists and is unique.*

Proof. Let f be an arbitrary function on \mathcal{H} , and define a function $g(x) = \sup\{\mu \mid (x, \mu) \in \text{conv}(\text{hypo } f)\}$. We show below that this g is the desired concave hull. We first show that g is concave. For any points $x, y \in \mathcal{H}$, if $\alpha < g(x)$ and $\beta < g(y)$, there exist $\varepsilon > 0$ such that $\alpha + \varepsilon < g(x)$ and $\beta + \varepsilon < g(y)$. Then, $((1 - \lambda)x + \lambda y, (1 - \lambda)\alpha + \lambda\beta + \varepsilon) \in \text{conv}(\text{hypo } f)$ for any $\lambda \in (0, 1)$. This leads to $g((1 - \lambda)x + \lambda y) > (1 - \lambda)\alpha + \lambda\beta$, thus showing that g is indeed concave. Also, by definition, g is minorized by f . The minimality of g follows from the minimality of a convex hull of sets. The uniqueness is obvious from the minimality. \square

An important implication of the proof of the Lemma 1 is how to derive the concave hull of a function: calculate the convex hull of its hypograph, and take the supremum. In the remaining sections, our interest is in cases where the function can be written in the following form:

$$f_y(x) = \begin{cases} y_i & \text{if } x = X_i, \\ -\infty & \text{otherwise.} \end{cases} \quad (3)$$

In this case, the hypograph of the function f_y is the set of vertical half-lines:

$$\text{hypo } f_y = \{(X_i, \mu) \mid \mu \leq y_i, i = 1, \dots, N\}. \quad (4)$$

In the Euclidean case, the convex hull of this set is characterized by the convex combination of the N points X_1, \dots, X_N , resulting in the concave hull of f being a piecewise linear function. However, in Hadamard spaces, the convex combination of N points is not well defined in that associativity does not hold. What we know is that Lemma 1 implies that any points (x, μ) in the convex hull of this set can be obtained by repeatedly taking the convex combination of two points. We use the notation $h_y = \text{conc } f_y(x)$ to denote this concave hull. We refer to function h_y as the *least concave function* with $h_y(X_i) \geq y_i$ ($i = 1, \dots, n$).

Also, note that as in the Euclidean case, the restrictions of convex (resp. concave) functions to a convex set are also convex (resp. concave). This is again because the intersection of two convex sets is also convex, so the hypograph of a restricted function is also convex. Following the usual convention in convex analysis, we regard a concave function f that has

as its domain some convex set $S \subseteq \mathcal{H}$ as a function on the whole of space \mathcal{H} which takes $-\infty$ outside S .

Another condition that is usually assumed with concavity is *upper-semicontinuity*. A function $f : \mathcal{H} \rightarrow [-\infty, \infty]$ is *upper-semicontinuous* at x if $\limsup_{y \in \mathcal{H}: d(x,y) \rightarrow 0} f(y) \leq f(x)$. If function f is upper-semicontinuous at all points $x \in \mathcal{H}$, then it is upper-semicontinuous on \mathcal{H} . It is also equivalent to the hypograph of f being closed.

Similar to concave hulls, we can define an *upper-semicontinuous hull* of a function f as the least upper-semicontinuous function minorized by f . That this function exists follows from the fact that (possibly infinite) intersections of closed sets are closed. Furthermore, it is possible to define the *upper-semicontinuous concave hull* of a function of f , as the least upper-semicontinuous concave function minorized by f . Concretely, this function is derived by taking intersections of the hypographs of all upper-semicontinuous and concave functions minorized by f . It can also be characterized as the function whose hypograph is $\text{cl}(\text{conv hypo} f)$. We denote the upper-semicontinuous concave hull of the function f_y by \bar{h}_y .

2.4 Probability Measure on Tree Space

In this section, we introduce one of the possible constructions of a probability measure on tree space. This construction is due to Willis (2019).

Let (\mathcal{T}_n, d) be tree space. Note that this space consists of $(2n - 3)!!$ Euclidean $(n - 2)$ -dimensional nonnegative orthants. Using this, one can write any set A in \mathcal{T}_n as a union of Euclidean sets, $A = \cup_{i=0}^{(2n-3)!!} A_i$. Here, A_0 denotes the set of trees in A that are also in the boundary of \mathcal{T}_n , and A_i denotes the set of trees in A that are also in the i -th positive orthant. Now, let ν_B be the Lebesgue measure on \mathbb{R}^{n-2} , and define ν by $\nu(A) = \sum_{i=1}^{(2n-3)!!} \nu_B(A_i)$. Then this ν preserves sigma additivity, and by completion of measures, ν becomes a complete measure.

In the remaining sections, we will use measure ν as a base measure and consider densities with respect to it.

3 Existence and Uniqueness of Maximum Likelihood Estimator

3.1 One-Dimensional Case

In this section, we consider the simplest tree space, \mathcal{T}_3 . Let \mathcal{F}_0 be the set of log-concave probability densities with respect to the base measure ν on this space. The following theorem indicates that maximum likelihood estimation in \mathcal{T}_3 could be performed in the same manner as in the Euclidean case.

Theorem 3. *Let (X_1, \dots, X_n) be an independent sample from $f \in \mathcal{F}_0$ in \mathcal{T}_3 , with $n \geq 2$. Then, with probability 1, the maximum likelihood estimator \hat{f}_n of f exists and is unique: i.e., \hat{f}_n is the unique maximizer in \mathcal{F}_0 of the log-likelihood function $l(f) = \sum_{i=1}^n \log f(X_i)$.*

The proof is given in the supplementary material.

Remark. Although our main interest is in tree space, it is simple to see that the above argument also applies to the space of $N \in \mathbb{N}$ half-lines connected at the origin.

3.2 Multidimensional Case

In this section, we consider the general p -dimensional tree space, \mathcal{T}_{p+2} . We let $\bar{\mathcal{F}}_0$ be the set of upper-semicontinuous log-concave densities in \mathcal{T}_{p+2} and $l(f) = \sum_{i=1}^n \log f(X_i)$ denote the log-likelihood function. The maximum likelihood estimator in this case, unlike in the cases of the one-dimensional tree space and Euclidean space, might not even exist. Before deriving a sufficient condition for the existence of the MLE, we first show that when the maximizer exists, its uniqueness can be stated as in the following theorem.

Theorem 4. *Let (X_1, \dots, X_n) be a sample from some density on \mathcal{T}_{p+2} . Suppose that a maximizer of $l(f)$ in $\bar{\mathcal{F}}_0$ exists. Then the maximizer is unique ν -almost everywhere.*

Proof. Suppose $f_1, f_2 \in \bar{\mathcal{F}}_0$ both maximize $l(f)$. If we put

$f(x) = \{f_1(x)f_2(x)\}^{1/2} / \int_{\mathcal{T}_{p+2}} \{f_1(z)f_2(z)\}^{1/2} d\nu(z)$, f is log-concave and

$$\begin{aligned} l(f) &= \frac{1}{2n} \sum_{i=1}^n \{\log f_1(X_i) + \log f_2(X_i)\} - \log \int_{\mathcal{T}_{p+2}} \{f_1(z)f_2(z)\}^{1/2} d\nu(z) \\ &\geq l(f_1) - \log \int_{\mathcal{T}_{p+2}} \frac{f_1(z) + f_2(z)}{2} d\nu(z) = l(f_1). \end{aligned} \quad (5)$$

Here, the last inequality is the relationship between the arithmetic mean and geometric mean, and equality holds if and only if $f_1(z) = f_2(z)$ ν -a.e.. \square

The next theorem provides a sufficient condition for sample points such that the maximum likelihood estimator exists and is unique almost everywhere.

Theorem 5. *Let (X_1, \dots, X_n) be a sample from a density f on \mathcal{T}_{p+2} , $n \geq p + 1$. Let $C_n = \text{conv}\{X_1, \dots, X_n\}$, and suppose that in each nonnegative orthant $\{O_i\}_{i=1}^{(2p+1)!!}$, one of the following conditions holds:*

- (a) $\text{cl}(C_n) \cap O_i$ does not contain any points.
- (b) $\text{cl}(C_n) \cap O_i$ constitutes a p -dimensional set in O_i : i.e., $\nu(C_n \cap O_i) > 0$.
- (c) $\text{cl}(C_n) \cap O_i$ only includes points at the boundaries, say B_j ($j = 1, \dots, J$), and each B_j is connected to at least one orthant O_j in which (b) holds.

Then, a maximum likelihood estimator \hat{f}_n of f in $\bar{\mathcal{F}}_0$ exists: i.e., $\hat{f}_n \in \bar{\mathcal{F}}_0$ is a maximizer of the log-likelihood function $l(f) = \sum_{i=1}^n \log f(X_i)$. Moreover, it is unique except in some set of ν -measure zero excluding $\text{int}(C_n)$.

Note that the sufficient condition is a condition that holds with a probability approaching one as n goes to infinity. Also, observe that this condition is easy to check if the convex hull of samples in \mathcal{T}_{p+2} can be calculated.

The proof is given in the supplementary material. In the proof of Theorem 3 and Theorem 5, it is shown that the maximum likelihood estimator of n samples are parametrized by n -dimensional vector $y \in \mathbb{R}^n$. Concretely, the logarithm of the maximum likelihood estimator \hat{f}_n is written in the form \bar{h}_y , the least upper-semicontinuous concave function with $h_y(X_i) \geq y_i$. Note that in one-dimensional case, the least concave function is upper-semicontinuous; i.e. $h_y = \bar{h}_y$. It is also shown that we need to maximize the objective

function $\psi_n(y)$ defined as follows:

$$\psi_n(y) = n^{-1} \sum_{i=1}^n \bar{h}_y(X_i) - \int_{\mathcal{T}_{p+2}} \exp(\bar{h}_y)(x) d\nu(x). \quad (6)$$

We also see in the proof that in some cases, the addition of a new point outside the existing convex hull does not induce an increase in the measure of the convex hull of the new set of points. Next is an example.

Example 6 (nonuniqueness). Consider that we have three points $X_1, X_2, X_4 \in \mathcal{T}_4$ as depicted in Figure 2. Then $\text{conv}\{X_1, X_2, X_4\}$ is the triangle $X_1X_2X_4$. Suppose that we add X_3 and consider $\text{conv}\{X_1, X_2, X_4, X_3\}$. Then this set is the union of triangle $X_1X_2X_4$ and the segment X_4X_3 , and it is clear that the measure has not increased: i.e., $\nu(\text{conv}\{X_1, X_2, X_4\}) = \nu(\text{conv}\{X_1, X_2, X_4, X_3\})$. Suppose that we have obtained $f \in \bar{\mathcal{F}}_0$ that satisfies $f(x) > 0$ ($x \in \text{conv}\{X_1, X_2, X_4\}$), $f(x) = 0$ ($x \notin \text{conv}\{X_1, X_2, X_4\}$). Then “extending” the support of f to include the segment X_3X_4 preserving log-concavity would not change the value of the likelihood function, and the extension of f would also be a density. Thus, ν -almost sure uniqueness holds, but strict uniqueness does not hold in this case.

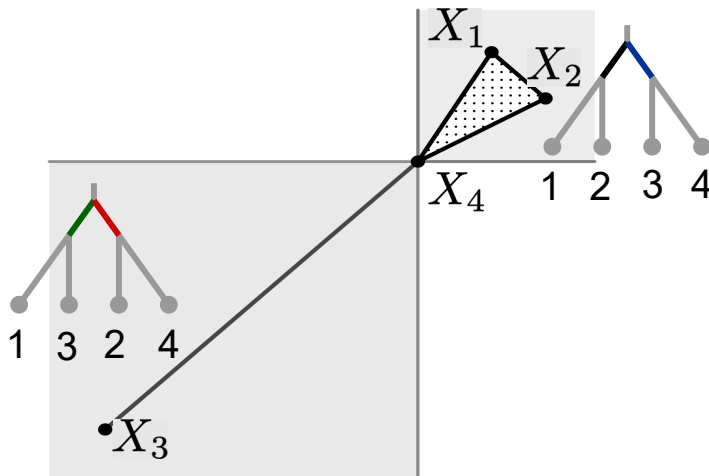


Figure 2: Illustration of Example 6 and Example 7. The two trees depicted are the topologies that the two orthants represent. Geodesics between these orthants are always cone paths.

Cases in which the maximum likelihood estimator does not exist occur when the convex hull has a measure-zero intersection with some orthant.

Example 7 (nonexistence). Consider that we have three samples $X_1, X_2, X_3 \in \mathcal{T}_4$ as depicted in Figure 2. The geodesics between points in these two trees necessarily are cone paths. It is clear that the assumption in Theorem 5 is not satisfied. Now, assume that the lengths of segments X_1X_4 and X_2X_4 are the same, and the length of segment X_3X_4 is three times that of X_1X_4 and X_2X_4 . Let $\log f$ be an affine-like function with $\log f(X_3) = y + \Delta$ and $\log f(X_2) = \log f(X_1) = y - \Delta/3$. Then $\log f(X_4) = y$ and

$$\psi_n(f) = y + \frac{\Delta}{9} - \int_C f(x)dx. \quad (7)$$

One can see that as Δ goes to $+\infty$ the second term linearly goes to $+\infty$ and the last integral term converges to zero. Thus, ψ_n is a monotone increasing function with respect to Δ and does not attain a maximum. Therefore, the maximum likelihood estimator does not exist in this case.

3.3 Densities That Bend at the Boundary

Although the nonparametric class of log-concave densities seem to be large enough to model various densities, there are densities that arise naturally, and are slightly not log-concave. In this section, we focus on the simplest one-dimensional tree space \mathcal{T}_3 , and discuss a way to incorporate densities that are not log-concave at the boundary. Let O_1, O_2, O_3 represent the three half-lines, and let the restriction of a density $f : \mathcal{T}_3 \rightarrow \mathbb{R}$ to each half-line O_i be f_i , which is a function on $\mathbb{R}_{\geq 0}$. Denote the exterior derivative at the origin by $\partial f_i / \partial n_i(0)$, defined as:

$$\frac{\partial f_i}{\partial n_i}(0) = \lim_{h \rightarrow +0} \frac{f_i(0) - f_i(h)}{h}. \quad (8)$$

Nye et al. (2014) considered diffusion process on \mathcal{T}_3 and defined a natural generalization of Gaussian density as a solution to the heat equation. If diffusion starts from the point $x_0 \in \mathbb{R}_{>0}$ in the orthant O_1 , the probability density at time t in each orthant can be written as follows:

$$\begin{aligned} f_1(x) &= \phi(x; x_0, t) - \frac{1}{3}\phi(x; -x_0, t) \\ f_j(x) &= \frac{2}{3}\phi(x; -x_0, t) \quad (j \in \{2, 3\}) \end{aligned} \quad (9)$$

Here, $\phi(x; \mu, \sigma^2)$ denotes the probability density function of normal distribution on \mathbb{R} with mean μ and variance σ^2 .

Density (9) does not have log-concavity since it “bends” at the origin. In fact, the exterior derivatives are

$$\begin{aligned} \frac{\partial f_1}{\partial n_1}(0) &= -\frac{4}{3}\phi'(0; x_0, t), \\ \frac{\partial f_j}{\partial n_j}(0) &= \frac{2}{3}\phi'(0; x_0, t) \quad (j \in \{2, 3\}). \end{aligned} \tag{10}$$

This makes density f to be not log-concave around the origin.

Another example can be constructed by considering a simple coalescent process of three lineages from three different species.

Example 8. Consider the species tree drawn on the left of Figure 3, and that three lineages are drawn from three species. In a neutral coalescent process (Kingman, 1982) with n lineages, the distribution of time that takes for any two lineages to coalesce is given by simple exponential distribution:

$$p(t) = \binom{n}{2} \exp\left(-\binom{n}{2}t\right) \tag{11}$$

In a multispecies coalescent (Rannala and Yang, 2003), one assume that the two lineages coalesce only after the corresponding two species coalesce. Let T be the time where exactly two clades of species exist as shown in the Figure 3. We can write the distribution of the length of internal edges by

$$f_i(x) = \begin{cases} -\frac{1}{6} \exp(-x - T) + \frac{1}{2} \exp(-x + T - 2 \max(0, T - x)) & \text{if } i = 1 \\ \frac{1}{3} \exp(-T - x) & \text{if } i \in \{2, 3\}, \end{cases} \tag{12}$$

where i denotes an index of orthant. See the supplementary material for the derivation.

This density is illustrated in Figure 3 for the case $T = 1$. We can clearly see that it is not log-concave. In fact, the exterior derivative is

$$\frac{\partial f_i}{\partial n_i}(0) = \begin{cases} -\frac{2}{3} \exp(-T) & \text{if } i = 1 \\ \frac{1}{3} \exp(-T) & \text{if } i \in \{2, 3\} \end{cases} \tag{13}$$

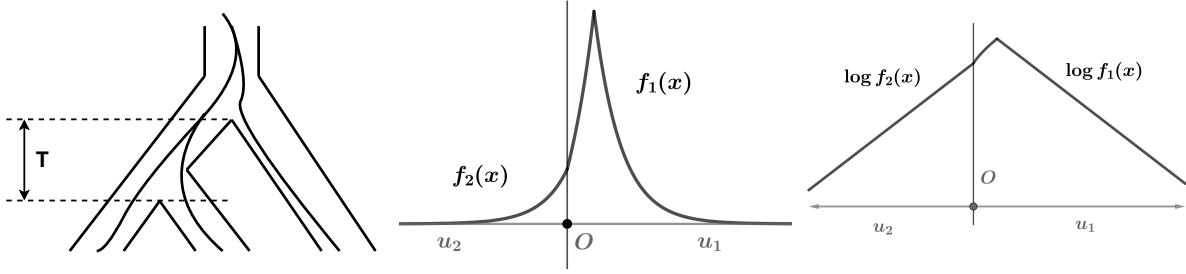


Figure 3: (Left): An example of how three lineages inside a species tree coalesce. T represents the length of internal edge in the species tree. (Center): The probability density in the orthants O_1 and the orthant O_2 . (Right): The logarithm of the probability density in the orthants O_1 and O_2 .

In these two examples, densities restricted to each half-line $\mathbb{R}_{\geq 0}$ are log-concave. The only non log-concave part is at the origin, where the absolute value of the slope of density differs. Concretely, the following relationship holds:

$$\frac{\partial f_1}{\partial n_1}(0) \leq 0, \quad \frac{\partial f_1}{\partial n_1}(0) = -2 \frac{\partial f_j}{\partial n_j}(0) \quad j \in \{2, 3\}. \quad (14)$$

We can also see that it satisfies the following Kirchhoff-type condition:

$$\sum_{i=1}^3 \frac{\partial f_i}{\partial n_i}(0) = 0. \quad (15)$$

These densities that bend at the origin can be incorporated in the model. We relax convexity condition of $\text{hypo}(\log f)$ to be the following:

1. $\text{hypo}(\log f) \cap O_i \times \mathbb{R}$ is convex for all $i \in \{1, 2, 3\}$
2. For $x_1 \in O_i$ and $x_2 \in O_j$ with $i \neq j$, let $\lambda = d(x_1, 0)/d(x_1, x_2)$, and

$$y_0 = \min \left\{ \frac{2(1-\lambda) \log f(x_1) + \lambda \log f(x_2)}{2-\lambda}, \frac{(1-\lambda) \log f(x_1) + 2\lambda \log f(x_2)}{1+\lambda} \right\}. \quad (16)$$

Then, $(0, y_0) \in \text{hypo}(\log f)$

We denote by \mathcal{G}_0 the class of densities which satisfy these two conditions. Any log-concave density f satisfies these two conditions since $y_0 \leq (1-\lambda)f(x_1) + \lambda f(x_2)$. Also, this allows for the bending at the origin to certain extent. In fact, the two densities we considered in this section is included in \mathcal{G}_0 .

We can now exploit similar arguments to the one-dimensional log-concave case in section 3.1 and derive the existence and uniqueness of the maximum likelihood estimator in \mathcal{G}_0 . Note that the resulting estimator does not require Kirchoff-type condition.

4 Calculation of Maximum Likelihood Estimator in One and Two Dimensions

For the maximization of the function ψ_y , we need to be able to calculate h_y for a given input vector y . In the one-dimensional case, this problem is reduced to the calculation of the convex hull of points $\{(X_1, y_1), \dots, (X_n, y_n)\}$. We explain below that this can be reduced to convex hull calculation in \mathbb{R}^2 , and the algorithm to calculate the log-concave maximum likelihood estimator is implementable.

In the two-dimensional case, the calculation of \bar{h}_y requires an algorithm to find the closure of the convex hull of points $\{(X_1, y_1), \dots, (X_n, y_n)\}$ in $\mathcal{T}_4 \times \mathbb{R}$. It is not known if we can obtain such algorithm, but we show below that obtaining an approximate convex hull is possible.

4.1 Calculation of the Least Concave Functions on \mathcal{T}_3

In order to obtain the maximum likelihood estimator (MLE), we need to be able to calculate the concave hull h_y of a function of the following type:

$$f_y(x) = \begin{cases} y_i & \text{if } x = X_i, \\ -\infty & \text{otherwise.} \end{cases} \quad (17)$$

As discussed in section 2.3, concave hulls can be found by first taking the convex hull of the hypograph and then taking the supremum. In this case, the problem is to find the convex hull D_n of a finite set of sample points in $\mathcal{T}_3 \times \mathbb{R}$.

\mathcal{T}_3 is a space consisting of three half-lines $\mathbb{R}_{\geq 0}$ connected at the origin. If all sample points are from one orthant, then the situation is the same as the Euclidean case, so we consider the case that the sample points are from at least two orthants. Let $y_0 = \max\{(1 - \lambda)y_i + \lambda y_j \mid i, j \in \{1, \dots, n\}, \lambda \in [0, 1], \gamma_{X_i, X_j}(\lambda) = 0\}$. Then, $(0, y_0)$ needs to

be in the convex hull D_n . Furthermore, if we take convex hull of sample points in each orthant including $(0, y_0)$ and take their union, this set, say E_n , becomes a convex set. Obviously E_n is included in D_n , thus by minimality of convex hulls, this set E_n in fact equals D_n . Since y_0 can be calculated by taking geodesics of all pairs of sample points, one can calculate D_n easily using the convex hull algorithm in Euclidean space \mathbb{R}^2 .

Similar arguments hold if we allow for the bend at the origin as discussed in the section 3.3. Concretely, we only need to alter the definition of y_0 to be

$$y_0 = \max \left\{ \min \left\{ \frac{\lambda y_j + 2(1 - \lambda)y_i}{2 - \lambda}, \frac{2\lambda y_j + (1 - \lambda)y_i}{1 + \lambda} \right\} \mid i < j, \lambda \in [0, 1], \gamma_{X_i, X_j}(\lambda) = 0 \right\}.$$

4.2 Approximation of \bar{h}_y on \mathcal{T}_4

In the two-dimensional case, it is not even known whether the convex hull of a finite number of points is closed. Recently, Lubiw et al. (2020) constructed an algorithm to find the closure of the convex hull of a finite number of points in single-vertex 2D CAT(0) complexes, including tree space, utilizing linear programming. Although we cannot transfer the algorithm directly to the product space of \mathcal{T}_4 and \mathbb{R} , Lubiw et al. (2020) also showed that by iteratively updating the values at the boundaries, one can construct a sequence of sets that converge to the desired convex hull. With a slight modification to this argument, as we show below, we can also create a similar situation so that by stopping at some iteration number, we can obtain an approximation of the convex hull.

To see this, let S_0 be all the sample points $\{(X_i, y_i) \mid X_i \in \mathcal{T}_4, y_i \in \mathbb{R}\}$. For simplicity, we will only consider the situation where the origin is in the convex hull (if the convex hull of sample points does not contain the origin, then the situation is the same as the Euclidean case). We call a geodesic in the space $\mathcal{T}_4 \times \mathbb{R}$ a cone path if it crosses the point of the type $\{0, y_l\}$, where 0 denotes the origin in \mathcal{T}_4 : that is, we call a geodesic a cone path when its projection onto \mathcal{T}_4 is a cone path. Also, for any nonnegative orthant O in \mathcal{T}_4 , define $S_0(O) = S_0 \cap (O \times \mathbb{R})$, $H_0(O) = \text{conv}(S_0(O))$ and $H_0 = \cup_O H_0(O)$. Following the terminology of Lubiw et al. (2020), we define the sets $S_l \subseteq \mathcal{T}_4 \times \mathbb{R}$ ($l = 0, 1, 2, \dots$) (which Lubiw et al. (2020) call the l -th skeletons) and $H_l \subseteq \mathcal{T}_4 \times \mathbb{R}$ ($l = 0, 1, 2, \dots$) iteratively as follows.

First, we take geodesics between points in H_{l-1} that are cone paths and find the val-

ues at the origin, which can be represented as $(0, y_{l,k})$. Then we find maximum and minimum values of $\{y_{l,k}\}$, and let them be y_{l1}, y_{l0} , respectively. We initialize T_l with $S_{l-1} \cup \{(0, y_{l1}), (0, y_{l0})\}$. Although it is practically difficult to find the exact maximum and minimum values, we can use an approximation algorithm. We discuss on this approximation in the supplementary material.

Now for each pair of points in T_l , take the geodesic between them, and add all intersection points with the boundaries to T_l . Here, by a boundary, we mean a two-dimensional plane formed by an axis on \mathcal{T}_4 and \mathbb{R} . Then, for each boundary in \mathcal{T}_4 , take all points that are also in T_l , including points at the origin, which are of the form $(0, y_{li})$. Since each boundary is a two-dimensional plane, these points can be thought of as points in \mathbb{R}^2 , and we take the usual two-dimensional Euclidean convex hull in this space. Then discard any points that are not vertices of this convex hull from T_l , and define $S_l = T_l$. Further, let O be any nonnegative orthant in \mathcal{T}_4 and $S_l(O)$ be the points in S_l that are also in $O \times \mathbb{R}$. Define $H_l(O) = \text{conv}(S_l(O))$, which can be computed easily since $S_l(O)$ can be embedded into a nonnegative orthant in \mathbb{R}^3 , and $H_l = \cup H_l(O)$.

This construction is similar to the two-dimensional CAT(0) case (Lubiw et al., 2020), but the differences are that in this case, we have to determine the maximum and minimum values at the origin first, and instead of preserving only extreme points in a one-dimensional axis, we need here to save all the vertices in the convex hull of points on boundaries.

To validate the first step, we first show the following lemma.

Lemma 9. *If S_{l-1} is included in $\text{conv}(S_0)$, then so is S_l .*

Proof. $S_{l-1} \subseteq \text{conv}(S_0)$ indicates $H_{l-1} \subseteq \text{conv}(S_0)$, and thus $\text{conv}(H_{l-1}) \subseteq \text{conv}(S_0)$. By construction, $S_l \subseteq \text{conv}(H_{l-1}) \subseteq \text{conv}(S_0)$. \square

The next theorem ensures that H_l converges to $\text{conv}(S_0)$.

Theorem 10. *Assume $p, q \in H_{l-1}$. Then the geodesic from p to q , denoted as $\gamma_{p,q}$, is included in H_l . This indicates that $\cup H_l = \text{conv}(S_0)$.*

Proof. If $\gamma_{p,q}$ is a cone path, let $(0, y_{0pq})$ be the point at which the geodesic crosses the origin. By construction, S_l includes points $(0, y_u)$ and $(0, y_l)$ such that $y_l \leq y_{0pq} \leq y_u$. Therefore, H_l includes $(0, y_{0pq})$, and thus all points of $\gamma_{p,q}$ are included in H_l .

If $\gamma_{p,q}$ is not a cone path, then the simplest case is that p, q are in the same orthant. In such a case, by construction, $\gamma_{p,q} \subseteq H_{l-1}$ as well. Thus, in particular, $\gamma_{p,q} \subseteq H_l$. Otherwise, let $p = (p_x, p_y), p_x \in \mathcal{T}_4, p_y \in \mathbb{R}$, and $q = (q_x, q_y), q_x \in \mathcal{T}_4, q_y \in \mathbb{R}$. We can take two nonnegative orthants $O_p, O_q \in \mathcal{T}_4$ to which p_x and q_x belong in such a manner that O_p and O_q are connected with at most one another orthant between them. Here, note that three connected orthants can be embedded in a part of \mathbb{R}^2 in the manner shown on the left of Figure 4. Now, we can take $a_p, b_p, c_p \in S_{l-1}(O_p)$ having the following property: the triangle $a_p b_p c_p$ includes the points of the form (p_x, y_{pp}) with $y_{pp} \geq p_y$. These points are the ones that form the triangle “over” point p . In the same way, we can take $a_q, b_q, c_q \in S_{l-1}(O_q)$ having the property that the triangle $a_q b_q c_q$ includes the points of the form (q_x, y_{qq}) with $y_{qq} \geq p_y$. The case when the triangles exactly include p and q are drawn in Figure 4. Let the intersection points of γ_{pq} with one of the boundaries, say B , be $r = (x_r, y_r)$. Also, in the Euclidean embedding of O_p, O_q , and B , as in Figure 4, let $-B$ denote the axis in the direction opposite to B (Figure 4). Recall that a “boundary” here means the Euclidean plane an axis in \mathcal{T}_4 makes in the space $\mathcal{T}_4 \times \mathbb{R}$. Consider embedded space \mathbb{R}^3 which includes O_p and O_q . If we allow paths to cross the part of the Euclidean space in which no orthants are embedded (the hatched region in Figure 4), it is easy to see from Euclidean geometry that we can find two straight lines between points in $\{a_p, b_p, c_p\}$ and $\{a_q, b_q, c_q\}$, say γ_1 and γ_2 , such that the line segment between the intersection points of γ_1 and γ_2 with B or $-B$, say $r_1 = (x_{r1}, y_{r1})$ and $r_2 = (x_{r2}, y_{r2})$, includes a point of the form (x_r, y'_r) with $y'_r \geq y_r$. If both r_1 and r_2 lie in B , then we just showed that $(x_r, y'_r) \in H_l$. If r_1 or r_2 does not lie in B , say r_1 does not, then we still find that the segment from r_1 to r_2 goes “under” $(0, y_{l1})$, since if we let $(0, y_{r1r2})$ be the origin point included in the segment $r_1 r_2$, then this point is included in some cone path between a point in the triangle $a_p b_p c_p$ and a point in the triangle $a_q b_q c_q$. Thus, the segment from $(0, y_{l1})$ to r_2 goes “over” (x_r, y'_r) : i.e., the segment includes a point of the form (x_r, y''_r) with $y''_r \geq y'_r \geq y_r$. Thus in summary, by setting either $\tilde{y}_r = y'_r$ or $\tilde{y}_r = y''_r$, we are able to find a point $(x_r, \tilde{y}_r) \in H_l$ such that $\tilde{y}_r \geq y_r$. A similar argument leads to that we can find a point $(x_r, \hat{y}_r) \in H_l$ such that $\hat{y}_r \leq y_r$. This indicates $r = (x_r, y_r) \in \mathcal{H}_l$, and consequently, the whole γ_{pq} .

□

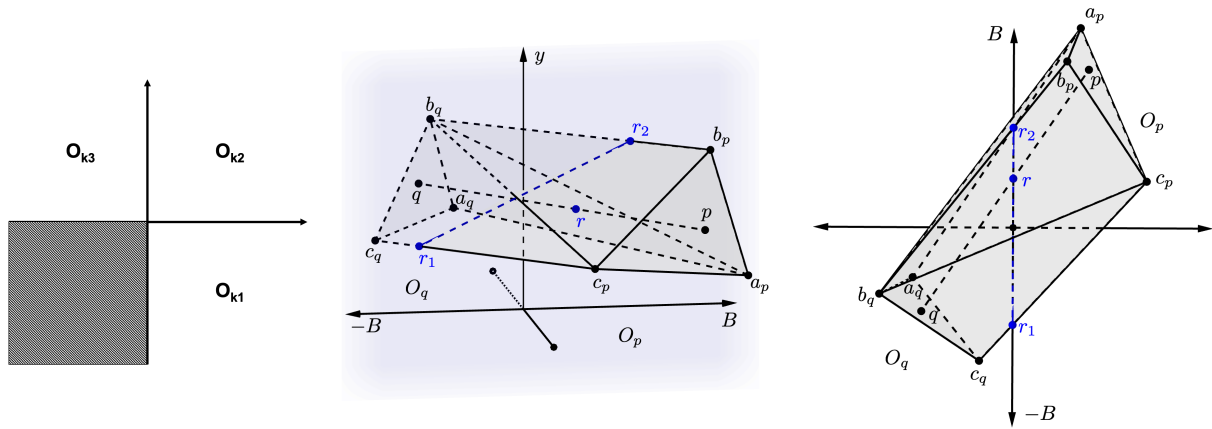


Figure 4: (Left): embeddings of three connected orthants to the Euclidean space \mathbb{R}^2 . (Center): an illustration that the path pq goes under the segment r_1r_2 . The three blue points are included in the blue plane. (Right): central figure seen from the direction of y -axis.

In Lubiw et al. (2020), a similar fact was revealed, and they proceed to reduce the problem of finding the closure of a convex hull to a linear programming problem. However, such a reduction is difficult in our case, given that we do not have prior knowledge about how many vertices $\text{conv}(S_0)$ would have on each boundary. We will content ourselves here with the approximation algorithm derived from the previous theorem. Note that if we can find maximum and minimum values at the origin exactly in the first step and the sets S_l converge in finite iteration number m , the set H_m is exactly equal to the desired convex hull. Furthermore, H_m is closed in this case, thus function \bar{h}_y calculated by this set is the exact least upper-semicontinuous concave function.

4.3 Altering the Objective Function

Sections 4.1 and 4.2 show that we can calculate the function \bar{h}_y for given y in one-dimensional and two-dimensional cases at least approximately. As shown at the beginning of this section, in order to find the maximum likelihood estimator, we need to solve the optimization problem of the form $\max_{y \in \mathbb{R}^n} \psi(\exp(h_y))$. As in the Euclidean case (Cule et al., 2010), the objective function is not a convex function of y , but by properly altering it, we can make this a convex optimization problem. In the d -dimension case, the new objective

function $\sigma_n(y)$ is defined as

$$\sigma_n(y) = -\frac{1}{n} \sum_{i=1}^n y_i + \int_{\mathcal{T}_{d+2}} \exp(h_y(x)) d\nu(x). \quad (18)$$

The convexity of \bar{h}_y with respect to y can be derived in exactly the same manner as in the Euclidean case (Cule et al., 2010). This ensures that σ is a convex function of y . Therefore, we can utilize ordinary solvers for convex optimization to calculate MLE.

5 Numerical Study

In this section, we give two simulation results. First, we show that the log-concave distribution can be estimated properly in one and two dimensions. We also test the estimation of one-dimensional density that bends at the origin. Then we compare this result with the kernel density estimator proposed by (Weyenberg et al., 2014). Finally, we give an example of clustering with the log-concave mixture model.

5.1 Estimation of One-Dimensional Log-Concave Densities

For one-dimensional examples, we consider the following two types of log-concave densities, using O_i ($i = 1, 2, 3$) to denote the three orthants in \mathcal{T}_3 .

Case 1. Normal-like density f_1 with mean equal to the point in O_1 that is 1 unit from the origin, x_0 : i.e., for a point $x \in \mathcal{T}_3$, $f_1(x) \propto \exp(-d(x, x_0)^2/2)$.

Case 2. Exponential-like density f_2 , defined as follows:

$$f_2(x) \propto \begin{cases} \exp(-d(x, x_0)) & \text{if } x \in O_2 \cup O_3 \text{ or } (x \in O_1 \text{ and } d(x, 0) < 1) \\ 0 & \text{otherwise.} \end{cases} \quad (19)$$

We generated ten samples each for sample size 100, 200, 300, 500, and 1000 from the true density and calculated the integrated squared error (ISE). The average ISE versus sample size is reported in Figure 5.

Our simulation results show that the log-concave MLE dominates the kernel density estimator for all sample sizes.

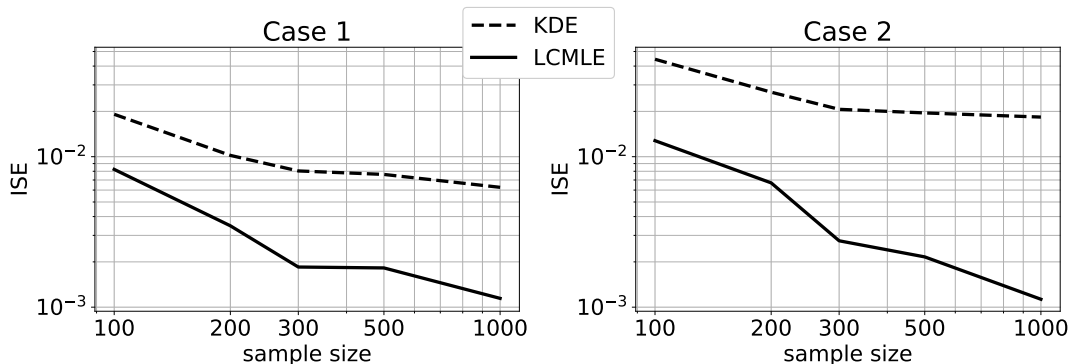


Figure 5: Average ISE for sample sizes 100, 200, 300, 500, and 1000 in case 1 (left) and case 2 (right). LCMLE denotes log-concave MLE, and KDE denotes kernel density estimator.

5.2 Estimation of Two-Dimensional Normal-like Densities

We denote each orthant of \mathcal{T}_4 by the indices of the axes at the boundary as in Figure 1. For instance, the orthant with axes 0 and 1 is denoted by $\{0, 1\}$. We consider densities of the following types:

Case 3. Positive truncated multivariate normal density f_3 with mean 0 and variance I , supported on all orthants in \mathcal{T}_4 :

$$f_3(x) \propto \exp(-d(x, 0)^2/2). \quad (20)$$

Case 4. Positive truncated multivariate normal density f_4 with mean 0 and variance I , supported on orthants

$\{0, 1\}, \{1, 6\}, \{6, 8\}, \{3, 8\}, \{3, 4\}, \{0, 4\}$:

$$f_4(x) \propto \begin{cases} \exp(-d(x, 0)^2/2) & \text{if } x \text{ is in one of the above orthants} \\ 0 & \text{otherwise.} \end{cases} \quad (21)$$

Also, because of the nonpositive curvature property of tree space, we have that these densities are log-concave.

We compare our log-concave MLE to the kernel density estimator (Weyenberg et al., 2014) in terms of ISE with respect to the true density. We generated ten samples each for sample size 50, 100, 200, 300, 500 and 1000 from the true density and calculated MLE and the average ISE. The estimation results are illustrated in Figure 6.

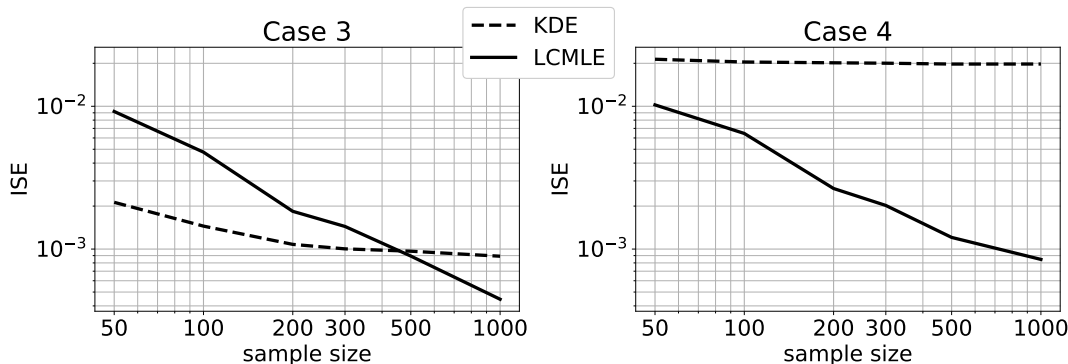


Figure 6: (Left) average ISE in case 3. (Right) average ISE in case 4. LCMLE denotes log-concave MLE, and KDE denotes kernel density estimator.

In case 3, the kernel density estimator performs better in small samples, but when a large number of samples are available, log-concave MLE starts to outperform the kernel density estimator. This result is similar to the Euclidean case (Cule et al., 2010). On the other hand, in case 4, log-concave MLE dominates the kernel density estimator. This is because while log-concave MLE can find the support of the true density with enough data, the kernel density estimator cannot.

5.3 Estimation of One-Dimensional Densities That Bend at the Origin

As one-dimensional densities that bend at the origin, we take two densities we considered in the section 3.3. Concretely, we consider the following two densities:

Case 5. Normal density constructed by Brownian motion f_5 at time 5 and starting position equal to the point in O_1 that is 1 unit away from the origin:

$$f_{5,1}(x) = \phi(x; 1, 5) - \frac{1}{3}\phi(x; -1, 5) \quad (22)$$

$$f_{5,j}(x) = \frac{2}{3}\phi(x; -1, 5) \quad (j \in \{2, 3\}) \quad (23)$$

Case 6. Density of coalescent time in Example 8 f_6 with $T = 1$: i.e., for a point $x \in \mathcal{T}_3$,

$$f_{6,1}(x) = -\frac{1}{6} \exp(-x - 1) + \frac{1}{2} \exp\{-x + 1 - 2 \max(0, 1 - x)\} \quad (24)$$

$$f_{6,j}(x) = \frac{1}{3} \exp(-x - 1) \quad j \in \{2, 3\} \quad (25)$$

As in the previous experiment with one-dimensional log-concave density, we generated ten samples each for sample size 100, 200, 300, 500 and 1000 from the true density and calculated MLE and the average ISE. The estimation results are illustrated in Figure 7.

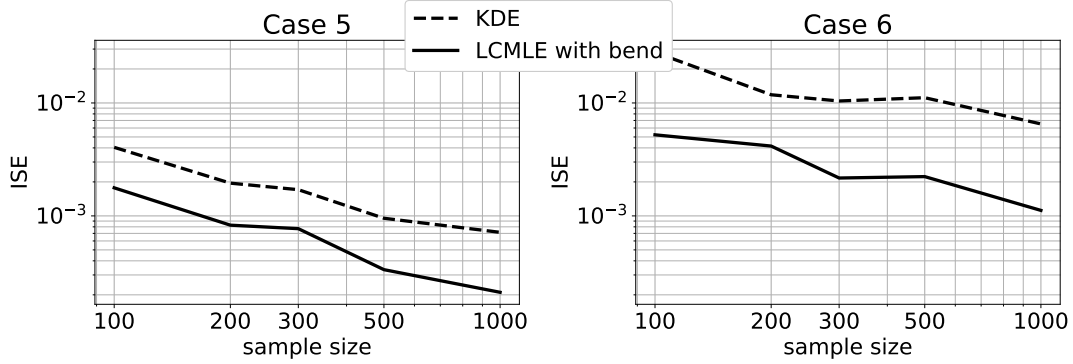


Figure 7: Average ISE for sample sizes 100, 200, 300, 500, and 1000 in case 5 (left) and case 6 (right). LCMLE with bend denotes MLE in \mathcal{G}_0 , and KDE denotes kernel density estimator.

The maximum likelihood estimator in \mathcal{G}_0 dominated the kernel density estimator for all sample sizes.

5.4 Clustering Example

In this section, we consider the problem of clustering in the space \mathcal{T}_4 . Let x_1 be a point in the orthant $\{0, 1\}$ and x_2 be a point in the orthant $\{2, 3\}$, both located at coordinates $(1, 1)$ in their orthant. We consider two normal-like densities on \mathcal{T}_4 , g_1 and g_2 , defined as follows:

$$g_1(x) \propto \exp(-d(x, x_1)^2/2), \quad (26)$$

$$g_2(x) \propto \exp(-2d(x, x_2)^2). \quad (27)$$

Note that g_1 and g_2 differ in variance as well as mean. We generated data from the mixture of g_1 and g_2 , $f = \pi_1 g_1 + (1 - \pi_1) g_2$ with proportion $\pi = 0.5$, and we attempted to cluster these points using log-concave MLE.

As in the Gaussian mixture in Euclidean space, we can construct an Expectation-Maximization algorithm (EM algorithm) to solve the clustering problem. We will assume that we know the number of clusters to be $K = 2$. We model the density in the following equation:

$$\hat{f} = \hat{\pi}_1 \hat{g}_1 + (1 - \hat{\pi}_1) \hat{g}_2, \quad (28)$$

where \hat{g}_1 and \hat{g}_2 are assumed to be log-concave. Cule et al. (2010) explained the EM algorithm applied to a log-concave density, and we adopt their framework here. Briefly, given data points X_i , the algorithm proceeds in the following way in the general case with K clusters. Given the current estimates of the mixture proportion and densities, $\hat{\pi}_k, \hat{g}_k$, the expectation step can be computed as

$$P(Z_i = k \mid X_i) = \frac{\hat{\pi}_k \hat{g}_k(X_i)}{\sum_{j=1}^K \hat{\pi}_j \hat{g}_j(X_i)}, \quad (29)$$

where $Z_i \in \{1, 2, \dots, K\}$ are the latent variables indicating the cluster the data come from. The maximization step is divided into two parts. First, for the estimate of \hat{f} , we maximize

$$\sum_{i=1}^n P(Z_i = k \mid X_i) \log g_k(X_i) \quad (30)$$

for each k to determine \hat{g}_k . The second part is the update of the mixture proportions, given by

$$\hat{\pi}_k = \frac{1}{n} \sum_{i=1}^n P(Z_i = k \mid X_i). \quad (31)$$

A subtle change in the optimization objective explained in section 4.3 will enable us to calculate the MLE in the maximization step. Concretely, it suffices to change the first term of equation (18) into the normalized version of equation (30):

$$\sum_{i=1}^n \frac{P(Z_i = k \mid X_i)}{\sum_{j=1}^n P(Z_j = k \mid X_j)} \log g_k(X_i). \quad (32)$$

The arguments thus far are still valid with this change.

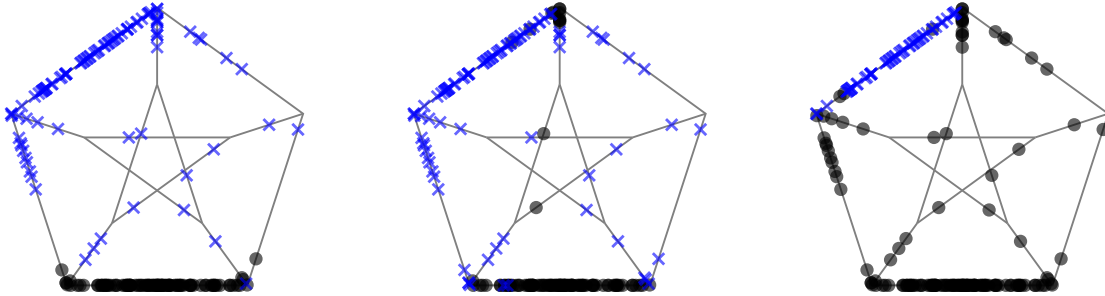


Figure 8: Clustered points displayed in the Petersen graph (Figure 1) with labels. (Left): data points with markers indicating the true clusters to which they belong. (Center): clustering results using the log-concave mixture (89% accuracy). (Right): clustering results using k-means++ (77 % accuracy). Note that closeness in this graph does not necessarily mean closeness in \mathcal{T}_4 .

To compare the results with other methods, we use the k-means++ algorithm (Vassilvitskii and Arthur, 2006) applied to this space as an alternative clustering method. Concretely, we implemented the usual k-means++ algorithm with the Fréchet mean instead of with the usual arithmetic mean. It is simple to see that the sum of squared distances from the cluster centers strictly decreases at each iteration of the k-means++ or k-means algorithm (MacQueen and Others, 1967) as in the Euclidean case. Thus the algorithm terminates within a finite number of steps.

The results of clustering are shown using the Petersen graph in Figure 8. We see from these results that in this case, the clusters estimated by the log-concave mixture estimate are more representative of the true density. This is a natural result, as the true density is indeed log-concave, and the two mixed normal densities have different variances.

6 Conclusion

In this paper, we showed that the maximum likelihood estimator exists in tree space under certain conditions. In one dimension, the maximum likelihood estimator exists with probability one and is unique, which is the same result as in the Euclidean case. In multiple-

dimension, there are conditions under which the MLE does not exist. However, if we restrict our attention to a particular situation, we have shown that the MLE exists and is unique ν -almost surely. Also, we have presented an algorithm to calculate the MLE exactly in the one-dimensional case and approximately in the two-dimensional case. We compared the results with the previously developed kernel density estimator and confirmed that our estimator dominates in well-modeled cases with a large enough sample size.

The method derived here is promising in that it gives a new nonparametric approach to density estimation on tree space. As we saw in a two-dimensional example, it is also able to respect the support of the sample distribution when it is convex, which might affect the estimation accuracy considerably in some situations. Unlike kernel density estimates, we do not need either the determination of smoothing parameters or the calculation of any (approximate) normalizing constant. Although the computation is much slower than kernel density estimates, the accuracy of density estimation can be expected to be high when the log-concavity assumption is not far away from the properties of the true density. The developed method gives an intermediate choice between fully unconstrained, nonparametric approaches, which have difficulties improving accuracy and estimation, and parametric approaches, for which it is difficult to specify the correct models for tree space.

For future research, it is important to derive some theoretical properties of the estimator on tree space. In Euclidean space, log-concave MLE is known to be strictly consistent, and even if the model is misspecified, it converges to the “log-concave projection” of the true density (the log-concave density that minimizes Kullback-Leibler divergence from the true density). It is crucial to investigate whether these properties hold on tree space as well. Also, It is of interest whether we can introduce different constraints on the density in order to include other types of densities on this space, or to lessen the computational load. The density that bend at the boundary, which we considered only in the one-dimensional case, is a candidate class for this purpose. Finally, further simulation studies in both well-modeled and misspecified cases are necessary for practical purposes.

As tree space is constructed for modeling the space of phylogenetic trees, one immediate interest of further research is the applicability to biological data and problems. As we only have (approximate) algorithms for one and two dimensions, corresponding to the case where a maximum of four taxa are present, the applicability seems to be limited for now.

However, it might be possible to seek lower-dimensional representations of large trees, for example, by grouping some taxa when they are irrelevant in terms of the inconsistency of multiple trees. It is of interest how well our method with these modifications performs compared to the existing methods with the biological data. Further careful assessment of the log-concavity assumption about the data distribution is also of interest. Furthermore, an attempt to improve computational efficiency is called for, as our method currently is not suited for use with large datasets.

Funding

This work was supported by JSPS KAKENHI Grant Number JP22J22685.

Maximum Likelihood Estimation of Log-Concave Densities on Tree Space : Supplementary Material

A Proofs of Theorem 5 and Theorem 3

In this section, we first derive some Lemmas related to the convex analysis in Hadamard spaces. Then we give a proof of Theorem 5, the existence of the maximum likelihood estimator in multi-dimensional cases. The proof of Theorem 3, the existence and uniqueness of the maximum likelihood estimator, follows similar arguments to the multi-dimensional cases (the proof of Theorem 5 and Theorem 4). Thus we only note the differences we need to consider.

A.1 Lemmas

First, we prepare some Lemmas. Let (\mathcal{H}, d) be a Hadamard space and for $i = 1, 2, \dots, n$, $(X_i, y_i) \in \mathcal{H} \times \mathbb{R}$. Let $D_0 = \{X_1, \dots, X_n\}$, and $C_n = \text{conv}(X_1, \dots, X_n)$. Lemma 1 suggests that this convex hull can be obtained by repeatedly taking geodesics starting from the set D_0 . Concretely, $C_n = \cup_{l=0}^{\infty} D_l$, where D_l consists of all points on the geodesics between points in D_{l-1} . We first show the boundedness of this convex hull.

Lemma 12. *Let $X_1, \dots, X_n \in \mathcal{H}$. Then $C_n = \text{conv}\{X_1, \dots, X_n\}$ is a bounded set.*

Proof of Lemma. This is proved using the nonpositive curvature property. By Lemma 1, $C_n = \cup_{l=0}^{\infty} D_l$, where $D_0 = \{X_1, \dots, X_n\}$ and D_l consists of all points that are on some geodesic with endpoints in D_{l-1} . Let $r = \max_{j=2, \dots, n} d(X_1, X_j)$. We can recursively show that for any points $x_l \in D_l$, $d(X_1, x_l) \leq r$. To see this, first note that at $l = 0$, the statement holds. Assuming that the statement holds at l , for any points $x_{l+1} \in D_{l+1}$, there exist $a_{l1}, a_{l2} \in D_l$ and $0 \leq \mu \leq 1$ such that $x_{l+1} = \mu a_{l1} + (1 - \mu) a_{l2}$. Then by CAT(0) inequality, $d(X_1, x_{l+1}) \leq \max_{k=1,2} d(X_1, a_{lk}) \leq r$. This shows the boundedness of C_n . \square

We say that \mathcal{H} has the *geodesic extension property* if any geodesic between two points in \mathcal{H} can be extended to a geodesic line. Now, we can show the following Lemma.

Lemma 13. *Suppose \mathcal{H} has the geodesic extension property. Then, any upper-semicontinuous concave function g on \mathcal{H} that is bounded in the domain S is continuous on $\text{int}(S)$.*

Proof. Let $g_{\text{int}(S)}$ denote the restriction of g to $\text{int}(S)$. Then, the hypograph of this function is $\{(x, \mu) \mid x \in \text{int}(S), \mu \leq g(x)\}$.

We first show that the interior of this set is given by $T = \{(x, \mu) \mid x \in \text{int}(S), \mu < g(x)\}$. That T includes $\text{int}(\text{hypo}g_{\text{int}(S)})$ is obvious. We only need to show that T is open. To see this, take any $(x, \mu) \in T$. Then there exists $\varepsilon_1 > 0$ such that $\mu + \varepsilon_1 = g(x)$. Because $x \in \text{int}(S)$, we can take $\varepsilon_2 > 0$ such that the closed ball $\bar{B}_{\varepsilon_2}(x) = \{y \in \mathcal{H} \mid d(x, y) \leq \varepsilon_2\}$ is included in $\text{int}(S)$. Now, take $\varepsilon_3 > 0$ to satisfy $\varepsilon_2 > \varepsilon_3$. Then, by the geodesic extension property, we can see that for any $\tilde{y} \in B_{\varepsilon_3}(x)$, there exists $y \in \text{int}(S)$ such that $d(x, y) = \varepsilon_2$ and for some $0 < \theta < 1$, $(1-\theta)x + \theta y = \tilde{y}$. Note that θ in the previous expression satisfies $\theta \leq \varepsilon_3/\varepsilon_2$. Because of concavity of g , $g(\tilde{y}) \geq g(x) - \theta(g(x) - g(y)) \geq g(x) - \varepsilon_3/\varepsilon_2(g(x) - g(y))$. Since g is bounded, by taking ε_3 sufficiently small, one can make for any $\tilde{y} \in B_{\varepsilon_3}(x)$, $g(\tilde{y}) > g(x) - \varepsilon_1/2$. Therefore, if we let $\varepsilon = \min\{\varepsilon_3, \varepsilon_1/2\}$, $B_\varepsilon(x) \subseteq T$. Thus, the set T is open.

For any $\alpha \in \mathbb{R}$, the intersection of two open sets $\text{int}(\text{hypo}(g_{\text{int}(S)}))$ and $\{(x, \mu) \mid \mu > \alpha\}$ is an open set $\{(x, \mu) \mid x \in \text{int}(C_n), g(x) > \mu > \alpha\}$, and thus the projection of this set $\{x \mid x \in \text{int}(C_n), g(x) > \alpha\}$. This implies the lower-semicontinuity, and thus the continuity, of g on $\text{int}(S)$. \square

Now, denote by Δ^{n-1} the $(n-1)$ -dimensional simplex in \mathbb{R}^n :

$$\Delta^{n-1} = \left\{ \lambda = (\lambda_1, \dots, \lambda_n) \in \mathbb{R}^n \mid \lambda_i \geq 0, \sum_{i=1}^n \lambda_i = 1 \right\} \quad (33)$$

For $\lambda \in \Delta^{n-1}$ and $l = 0, 1, \dots$, define sets $S_{\lambda, l}$ as follows:

$$S_{\lambda, 0} = \begin{cases} \{X_i\} & \text{if } \lambda_i = 1, \lambda_j = 0 \ (\forall j \neq i) \\ \emptyset & \text{otherwise} \end{cases} \quad (34)$$

$$S_{\lambda, l} = \{x \in D_l \mid \exists x_1 \in S_{\lambda_1, l-1}, \exists x_2 \in S_{\lambda_2, l-1}, 0 \leq \exists \mu \leq 1, \\ \gamma_{x_1, x_2}(\mu) = x, (1-\mu)\lambda_1 + \mu\lambda_2 = \lambda\} \quad (l = 1, 2, \dots).$$

Let $S_\lambda = \cup_{l=0}^{\infty} S_{\lambda, l}$. Informally, S_λ is the set of points which can be generated with cumulated coefficient of convex combination λ . Lemma 1 indicates that for any point $x \in C_n$, at least

one $\lambda \in \Delta^{n-1}$ exists such that $x \in S_\lambda$. This also implies that $\text{conv}(\{X_i, y_i\}_{i=1}^n)$ includes the point $(x, \lambda^\top y)$.

Let $y = (y_1, \dots, y_n)$ and denote by $f_y(x)$ the following function:

$$f_y(x) = \begin{cases} y_i & \text{if } x = X_i \\ -\infty & \text{otherwise.} \end{cases} \quad (35)$$

Let \bar{h}_y denote the upper-semicontinuous concave hull of f_y . Following two Lemmas show some properties of this function.

Lemma 14. $\bar{h}_y(x)$ is continuous with respect to $y = (y_1, \dots, y_n)$.

Proof. For any fixed value $x \in \mathcal{H}$, $\bar{h}_{y+\delta}(x)$ cannot deviate from $\bar{h}_y(x)$ by more than $\|\delta\|_2$.

In order to see this, first, assume $\bar{h}_{y+\delta}(x) \leq \bar{h}_y(x)$. By construction, the hypograph of \bar{h}_y is given by

$$\text{hypo } \bar{h}_y = \text{cl}(\text{conv}(\text{hypo } f_y)) \quad (36)$$

Let $\mu = \bar{h}_y(x)$. Equation (36) indicates that there exists $\{(x_i, \mu_i)\}_{i=1}^\infty \subseteq \text{conv}(\text{hypo } f_y)$ such that the sequence $\{(x_i, \mu_i)\}_{i=1}^\infty$ converges to (x, μ) . Furthermore, by Lemma 1, there exists $\lambda^{(i)} \in \Delta^{n-1}$ for each (x_i, μ_i) such that $x_i \in S_{\lambda^{(i)}}$ and $\mu_i \leq (\lambda^{(i)})^\top y$. This implies that $(x_i, (\lambda^{(i)})^\top (y + \delta)) \in \text{hypo}(\bar{h}_{y+\delta})$, $\mu_i - \|\delta\|_2 \leq (\lambda^{(i)})^\top (y + \delta)$, and thus $(x_i, \mu_i - \|\delta\|_2) \in \text{hypo}(\bar{h}_{y+\delta})$. Now, the sequence of points $\{(x_i, \mu_i - \|\delta\|_2)\}_{i=1}^\infty$ converges to $(x, \mu - \delta)$, and this points is included in $\text{hypo}(\bar{h}_{y+\delta})$ by the upper-semicontinuity. This shows that $\bar{h}_{y+\delta}(x) \geq \mu - \|\delta\|_2$ and consequently, $\bar{h}_y(x) - \bar{h}_{y+\delta}(x) \leq \|\delta\|_2$.

If $\bar{h}_{y+\delta}(x) > \bar{h}_y(x)$, let $\mu = \bar{h}_{y+\delta}(x)$, and by interchanging the roles of \bar{h}_y and $\bar{h}_{y+\delta}$ in the above argument, we can show $\bar{h}_{y+\delta}(x) - \bar{h}_y(x) \leq \|\delta\|_2$. \square

Lemma 15. $\text{dom } \bar{h}_y = \text{cl}(C_n)$.

Proof. For any upper-semicontinuous concave function g satisfying $g(X_i) \geq y_i$, let the restriction of g to $\text{cl}(C_n)$ be $g_{\text{cl}(C_n)}$. Then $\text{hypo } g_{\text{cl}(C_n)} = \text{hypo } g \cap \{(x, \mu) \mid x \in \text{cl}(C_n), \mu \in \mathbb{R}\}$ is closed. This means that $g_{\text{cl}(C_n)}$ is upper-semicontinuous. Furthermore, since $X_i \in C_n$, $g_{\text{cl}(C_n)}(X_i) = g(X_i) \geq y_i$. With the minimality of \bar{h}_y , this implies that $\text{dom } \bar{h}_y \subseteq \text{cl}(C_n)$.

On the other hand, take any $x \in \text{cl}(C_n)$. Then there exists a sequence $\{x_i\}_{i=1}^\infty \subseteq C_n$ such that $x = \lim_{i \rightarrow \infty} x_i$. By the concavity of \bar{h}_y , $\bar{h}_y(x_i) \geq \min_{j=1,2,\dots,n} y_j$ for all $i = 1, 2, \dots$

By the upper-semicontinuity, $\min_{j=1,2,\dots,n} y_j \leq \lim_{i \rightarrow \infty} f(x_i) \leq f(x)$. This shows that $x \in \text{dom } \bar{h}_y$, and consequently, $\text{cl}(C_n) \subseteq \text{dom } \bar{h}_y$. \square

A.2 Proof of Theorem 5

Proof of theorem. The proof is essentially a modification of the proof of Theorem 1 from Cule et al. (2010).

By Lemma 1, $C_n = \cup_{l=0}^{\infty} D_l$, where D_l denotes the set defined in the proof of the previous Lemma. Let $\bar{\mathcal{F}}$ be the set of upper-semicontinuous log-concave functions on \mathcal{T}_{p+2} , and consider the maximization of the function $\psi_n(f) = n^{-1} \sum_{i=1}^n \log f(X_i) - \int_{\mathcal{T}_{p+2}} f(x) d\nu(x)$ over $\bar{\mathcal{F}}$.

First, we can show that for any $g \in \bar{\mathcal{F}}$, there exists $f \in \bar{\mathcal{F}}$ such that $\psi_n(f) \geq \psi_n(g)$ with

$$f(x) > 0 \ (x \in \text{cl}(C_n)), \quad f(x) = 0 \ (x \notin \text{cl}(C_n)). \quad (37)$$

First, assume $g(x) = 0$ for some $x \in C_n$. Lemma 1 suggests that there exists $l \in \mathbb{N}$ such that $x \in D_l$. If $l = 1$, we have for some k , $g(X_k) = 0$, implying $\psi_n(g) = -\infty$. Otherwise, take minimum such l , then one can take some $x_{1,l-1}, x_{2,l-1} \in D_{l-1}$ and $\mu \in (0, 1)$ such that $x = (1 - \mu)x_{1,l-1} + \mu x_{2,l-1}$. By concavity, $-\infty = \log g(x) \geq (1 - \mu) \log g(x_{1,l-1}) + \mu \log g(x_{2,l-1})$. This leads to that at least one of $g(x_{1,l-1})$ and $g(x_{2,l-1})$ must be zero. Repeating this process, we can show that there exists $k \in \{1, \dots, n\}$ such that $g(X_k) = 0$, resulting again in $\psi_n(g) = -\infty$. Therefore, if for some $x \in C_n$, $g(x) = 0$, then any f with (37) satisfies $\psi_n(f) \geq \psi_n(g)$. If $g(x) = 0$ for some $x \in \text{cl}(C_n) \setminus C_n$, then one can take a sequence $\{x_i\} \in C_n$ such that x_i converges to x . The upper-semicontinuity implies that $\limsup_{i \rightarrow \infty} g(x_i) \leq g(x) = 0$. Then for all $\varepsilon > 0$, there exists i such that $g(x_i) < \varepsilon$. This with the previous argument leads to that $\min_{k=1,\dots,n} g(X_k) < \varepsilon$. Since ε can be taken arbitrarily small, $\min_{k=1,\dots,n} g(X_k) = 0$, which leads again to $\psi_n(g) = -\infty$. On the other hand, because $\text{cl}(C_n)$ is bounded by Lemma 12, if we take $f \in \bar{\mathcal{F}}$ to be finitely positive and upper-semicontinuous on $\text{cl}(C_n)$, f becomes upper-semicontinuous on $\text{dom } f$ and $\psi_n(f) > -\infty$. Thus, we can strictly restrict our attention to f such that $f(x) > 0$ for all $x \in C_n$.

Now, assume that $g(x) > 0$ for some $x \notin \text{cl}(C_n)$. Then by letting $f(x)$ be the restriction of $g(x)$ to $\text{cl}(C_n)$, it is easy to see that f satisfies (37), log-concavity, and upper-semicontinuity. Furthermore, $\psi_n(f) \geq \psi_n(g)$, and the inequality becomes the strict one if $\nu(\{x \mid x \in \text{dom } g, x \notin C_n\}) > 0$. This means that we can strictly restrict attention to the density that satisfies (37), or the ones that satisfy them except for some set of ν -measure zero excluding $\text{cl}(C_n)$.

Secondly, we can show that for any upper-semicontinuous function g , there exists f which has its logarithm in the form \bar{h}_y such that $\psi_n(f) \geq \psi_n(g)$. This is achieved if we put $y_i = \log g(X_i)$, $y = (y_1, \dots, y_n)$ and $f = \exp(\bar{h}_y)$. Note that by Lemma 15, $\text{dom } \bar{h}_y = \text{cl}(C_n)$. Also, by Lemma 13, \bar{h}_y is continuous relative to $\text{int}(C_n)$. Because of continuity, if $g(x) \neq \exp(\bar{h}_y)(x)$ at some $x \in \text{int}(C_n)$, $\psi_n(\exp(\bar{h}_y)) > \psi_n(g)$. This shows that a maximizer of ψ_n , if it exists, has to take the form $\psi_n(\bar{h}_y)$ in $\text{int}(C_n)$.

Next, we can also show that we can restrict attention to the case $f \in \mathcal{F}_0$. For any upper-semicontinuous function g , assume $\int_{\mathcal{T}_{p+2}} g(x) = c < \infty$. By setting $f = g/c$, $f \in \mathcal{F}_0$,

$$\begin{aligned} \psi_n(f) &= \frac{1}{n} \sum_{i=1}^n \log f(X_i) - \int_{\mathcal{T}_{p+2}} f(x) d\nu(x) \\ &= \frac{1}{n} \sum_{i=1}^n \log g(X_i) - \log c - 1 \\ &= \psi_n(g) + c - \log c - 1 \\ &\geq \psi_n(g). \end{aligned} \tag{38}$$

Equality is attained only when $c = 1$.

For the existence of a maximizer of $l(f)$, it only remains to show that ψ_n has a maximizer $f = \exp(\bar{h}_y) \in \mathcal{F}_0$ with (37).

This is seen as follows. For an arbitrary function $f = \exp(\bar{h}_y)$ with (37), let $X_{\max} = \arg \max_{X_i} g(X_i)$ and O_{\max} be one of the nonnegative orthants of \mathcal{T}_{p+2} which X_{\max} belongs to. Then by assumption, $\nu(C_n \cap O_{\max}) =: V > 0$. Now, put $M = \bar{h}_y(X_{\max})$ and $m = \min_{x \in O_{\max}} \bar{h}_y(x)$. For sufficiently large M , $M - 1 > m$. Then by setting $\lambda = 1/(M - m)$, the concavity $\bar{h}_y(\lambda x + (1 - \lambda)X_{\max}) \geq \lambda \bar{h}_y(x) + (1 - \lambda)\bar{h}_y(x)$ indicates

$$\bar{h}_y \left(\frac{1}{M - m} x + \frac{M - m - 1}{M - m} X_{\max} \right) \geq \frac{m}{M - m} + \frac{(M - m - 1)M}{(M - m)} = M - 1.$$

This in turn indicates $\nu(\{x \mid \bar{h}_y(x) \geq M-1\}) \geq V/(M-m)^p$, and thus $1 = \int_{\mathcal{T}_{p+2}} \exp(\bar{h}_y(x)) d\nu(x) \geq V(\exp(M-1))/(M-m)^p$. Therefore,

$$\begin{aligned} M - m &\geq V^{\frac{1}{p}} (\exp(M-1))^{\frac{1}{p}} \\ \therefore m &\leq M - V^{\frac{1}{p}} \exp\left(\frac{M-1}{p}\right). \end{aligned} \quad (39)$$

This leads to the following inequality:

$$\begin{aligned} \psi_n(\exp(\bar{h}_y)) &= \frac{1}{n} \sum_{i=1}^n \bar{h}_y(X_i) - 1 \\ &\leq \frac{n-1}{n} M + \frac{M}{n} - \frac{V^{\frac{1}{p}}}{n} \exp\left(\frac{M-1}{p}\right) \\ &= M - \frac{V^{\frac{1}{p}}}{n} \exp\left(\frac{M-1}{p}\right) \end{aligned} \quad (40)$$

This inequality shows that as M goes to infinity, ψ_n goes to $-\infty$. On the other hand, because \bar{h}_y is continuous with respect to y , as shown in Lemma 14, $\psi_n(\exp(\bar{h}_y)) = n^{-1} \sum_{i=1}^n \bar{h}_y(X_i) - \int_{\mathcal{T}_{p+2}} \exp(\bar{h}_y)(x) dx$ is also continuous. Thus, there exists $r = \max_{y \in [-M, M]^n} \psi_n(\exp(\bar{h}_y))$. This shows the existence of a maximizer of $\psi_n(f)$, and thus $l(f)$.

The uniqueness of the maximizer in the ν -almost sure sense is guaranteed by Theorem 4. Moreover, by the previous argument, the maximizer needs to be the form $\exp(\bar{h}_y)$ for some $y \in \mathbb{R}^d$, in $\text{int}(C_n)$. Since \bar{h}_y is continuous in $\text{int}(C_n)$, the strict uniqueness in $\text{int}(C_n)$ holds. \square

A.3 Proof of Theorem 3

Proof. The proof goes in a similar way as in the proof of Theorem 5. Here, we note several properties specific to the one-dimensional case, which is necessary for the proof.

- $C_n = \text{conv}(X_1, \dots, X_n)$ is a closed bounded set. This, in particular, implies $\text{cl}(C_n) = C_n$. Thus the domain of the maximizer can be restricted to exactly C_n .
- The logarithm of the maximizer can always be written in the form h_y , the least concave function with $h_y(X_i) \geq y_i$. h_y is continuous on C_n .
- Because f is absolutely continuous with respect to ν , with probability 1, C_n is not merely a point, but constitutes an interval. This is essentially a substitute for the

sufficient condition (a)-(c) we considered in the multi-dimensional case. We can easily see that this condition is sufficient for showing that the maximizer of ψ_n exists in the set of densities of the form $\exp(h_y)$.

- The strict uniqueness follows from the following two observations: h_y is continuous on C_n , and the extension of the domain always provokes the increase in the measure.

□

B Derivation of distribution of 3-trees under coalescent

In this section, we derive the equation (13) in Example 8, the distribution of 3-trees generated from multi-species coalescent.

In order to consider the distribution on tree space, we need to consider the distribution of gene tree topology and the internal edge length given species tree. Algorithms for calculating gene tree topology given specific species trees have been considered in general dimension (Degnan and Salter, 2005; Wu, 2012), but the direct calculation is also available in small trees (e.g. Takahata and Nei, 1985; Pamilo and Nei, 1988). In the case of simplest case of 3-trees, denote by u_1 is the topology of the species tree and by u_2, u_3 the rest of the topologies. Then the distribution of gene tree topology U_g is given by:

$$\begin{aligned} P(U_g = u_1) &= 1 - \frac{2}{3}e^{-T}, \\ P(U_g = u_j) &= \frac{1}{3}e^{-T} \quad (j = 2, 3), \end{aligned} \tag{41}$$

where T denotes the length of the internal edge of the species tree.

Given U_g , the distribution of the internal edge length can be derived in the following manner. First, consider the cases where $U_g \neq u_1$. In these cases, the distribution of the internal edge length is the same as the distribution of the coalescence time of two lineages. Standard coalescent theory implies that the density of the internal edge length is given by

$$f(x | U_g = u_j) = \exp(-x). \tag{42}$$

Next, we consider the case $U_g = u_1$. Let τ denote the time of the first coalescence of any two lineages after the first coalescence of the species tree coalescence (Figure 9). Thus,

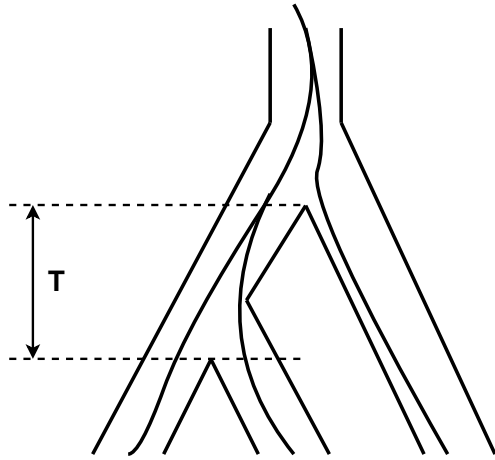


Figure 9: Illustration of coalescence of three lineages from three different species. τ denotes the time of the first coalescence of genes after the first coalescence of the species tree.

the value of τ being close to zero means that the two gene lineages coalesce right after the species tree coalesces, and the value of τ larger than T means that two gene lineages coalesce after whole three species coalesced in the species tree. Multi-species coalescent assumes that the coalescence is neutral. In terms of τ , this can be written as

$$P(U_g = u_1 | \tau) = \begin{cases} 1 & \text{if } \tau \leq T \\ \frac{1}{3} & \text{otherwise} \end{cases}. \quad (43)$$

When $\tau \leq T$, the density of τ is $\exp(-\tau)$. This, combined with the equation (43), implies that the conditional density of τ given $U_g = u_1$ for $\tau \leq T$ is given by

$$f(\tau | U_g = u_1) = \frac{1}{1 - (2/3)\exp(-T)} \exp(-\tau) \quad \text{if } \tau \leq T. \quad (44)$$

We can now calculate the density of the internal edge length x given $U_g = u_1$ as follows:

$$\begin{aligned}
& f(x | U_g = u_1) \\
&= \int_0^T f(x | U_g = u_1, \tau) f(\tau | U_g = u_1) d\tau + \int_T^\infty f(x | U_g = u_1, \tau) f(\tau | U_g = u_1) d\tau \\
&= \left(1 - \frac{2}{3} \exp(-T)\right)^{-1} \int_0^T \exp(-(x - (T - \tau))) \mathbb{1}(x \geq T - \tau) \exp(-\tau) d\tau \\
&\quad + \int_T^\infty \exp(-x) f(\tau | U_g = u_1) d\tau \\
&= \left(1 - \frac{2}{3} \exp(-T)\right)^{-1} \int_{\max\{0, T-x\}}^T \exp(-x + T) \exp(-2\tau) d\tau \\
&\quad + \exp(-x) \left\{1 - \int_0^T f(\tau | U_g = u_1) d\tau\right\} \\
&= \left(1 - \frac{2}{3} \exp(-T)\right)^{-1} \left\{-\frac{1}{2} \exp(-x + T) [\exp(-2\tau)]_{\max\{0, T-x\}}^T\right\} \\
&\quad + \frac{\exp(-T)}{3} \left(1 - \frac{2}{3} \exp(-T)\right)^{-1} \exp(-x) \\
&= \left(1 - \frac{2}{3} \exp(-T)\right)^{-1} \left[-\frac{1}{6} \exp(-x - T) + \frac{1}{2} \exp(-x + T - 2 \max\{0, T - x\})\right] \quad (45)
\end{aligned}$$

Equations (45), (41) leads to the equation (13) in Example 8.

C Bounds for maximum and minimum values at the origin generated by geodesics in H_{l-1}

As mentioned in the main text, finding the maximum and minimum values at the origin in the first step of this approximation algorithm is not a simple optimization problem. For example, the problem of finding the maximum value at the origin among all geodesics between points in two specific orthants, say O_1 and O_2 , can be written in the following

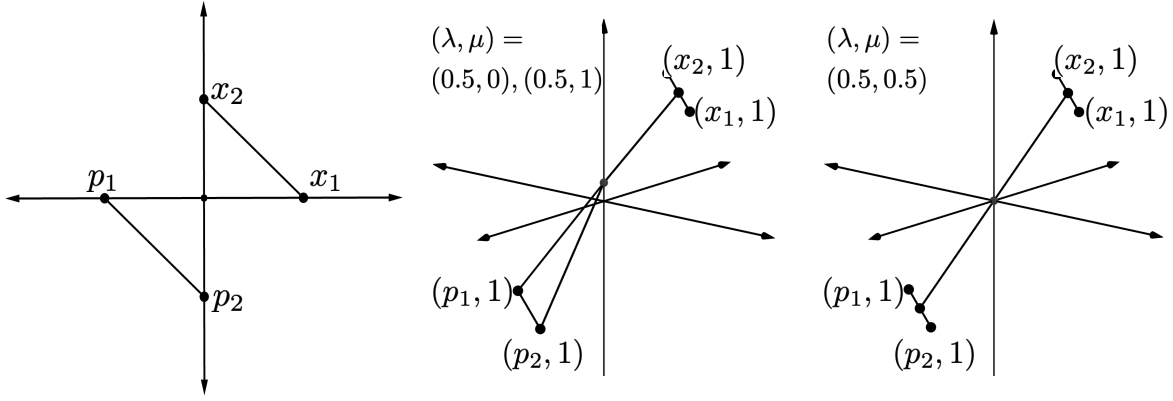


Figure 10: Points used in Example 16. (Left): four points x_1, x_2, p_1, p_2 . (Center): the optimal cone paths with $(\lambda, \mu) = (0.5, 1), (0.5, 0)$. (Right): the cone path when $(\lambda, \mu) = (0.5, 0.5)$.

way: given points $\{x_i, y_i\} \in O_1 \times \mathbb{R}$ and $\{p_j, q_j\} \in O_2 \times \mathbb{R}$,

$$\begin{aligned}
 & \max_{\mu_i, \lambda_j} \frac{\|\sum_i \mu_i x_i\| \|\sum_j \lambda_j q_j\| + \|\sum_j \lambda_j p_j\| \|\sum_i \mu_i y_i\|}{\|\sum_i \mu_i x_i\| + \|\sum_j \lambda_j p_j\|} \\
 & \text{s.t.} \quad \sum_i \mu_i = 1 \\
 & \quad \quad \sum_j \lambda_j = 1
 \end{aligned} \tag{46}$$

$$1 \geq \mu_i, \lambda_j \geq 0$$

the geodesic between $\sum_i \mu_i x_i$ and $\sum_j \lambda_j p_j$ is a cone path.

Although the last nonconvex constraint can be removed when we are considering some combinations of two orthants, the objective function is also nonconvex. The next is an example that shows nonconvexity in a very simple case.

Example 16. Consider two orthants O_1 and O_2 separated by two other orthants so that the geodesic between points in two orthants are necessarily cone paths. We assume that we have two points in each orthant, say $x_1 \in O_1, x_2 \in O_1, p_1 \in O_2, p_2 \in O_2$, with the coordinates at each orthant being $(0, 1), (1, 0), (0, 1), (1, 0)$ respectively. We consider the problem (46) with four points $(x_1, 1), (x_2, 1), (p_1, -1), (p_2, -1)$ (Figure 10).

Then the optimization problem to solve is

$$\begin{aligned} \max_{\mu, \lambda} \quad & f(\mu, \lambda) = \frac{-\sqrt{\mu^2 + (1 - \mu)^2} + \sqrt{\lambda^2 + (1 - \lambda)^2}}{\sqrt{\mu^2 + (1 - \mu)^2} + \sqrt{\lambda^2 + (1 - \lambda)^2}} \\ \text{s.t.} \quad & 1 \geq \mu, \lambda \geq 0 \end{aligned} \quad (47)$$

The optimal solutions to this problem are $(\lambda, \mu) = (0.5, 1)$ and $(\lambda, \mu) = (0.5, 0)$. Moreover, $(\lambda, \mu) = (0.5, 0.5)$ is a saddle point, and the second derivatives are

$$\frac{\partial^2 f}{\partial \mu^2} \Big|_{\mu=0.5, \lambda=0.5} = -2, \quad (48)$$

$$\frac{\partial^2 f}{\partial \lambda^2} \Big|_{\mu=0.5, \lambda=0.5} = 2. \quad (49)$$

Thus, the objective function is concave in μ and convex in λ around $(\mu, \lambda) = (0.5, 0.5)$.

As it is computationally intensive to solve this nonconvex optimization problem at each iteration, we replace the maximum (resp. minimum) values at the origin with its lower bound (resp. upper bound), which can be easily computed by linear programming. In the following paragraph, we explain the algorithm to calculate the replacement value.

First, note that in the two-dimensional tree space, there are 15 orthants, each consisting of two axes at a right angle, and each axis is connected to two other orthants. Thus, there are $15 \times 4 = 60$ combinations of three orthants connected sequentially, as one can see by Figure 1 in the main text. We denote these combinations of orthants as $\{(O_{k1}, O_{k2}, O_{k3})\}_{k=1}^{60}$, where O_{k1}, O_{k2}, O_{k3} are connected in this order.

Figure 4 in the main text is a valid representation of orthants O_{k1}, O_{k2}, O_{k3} in the Euclidean space, in the sense that the distance between two points in these orthants is respected if we do not allow the paths to cross the space outside these three orthants, which is the hatched region on the left in Figure 4. Then, the space $\cup_{j=1}^3 O_{kj} \times \mathbb{R}$ constitutes a part of \mathbb{R}^3 , as depicted on the right in Figure 4. For all 60 combinations of these orthants, we embed points of S_{l-1} in \mathbb{R}^3 , calculate the usual three-dimensional convex hull in this space (allowing paths to cross the quadrant which is not used for the embedding), and if the convex hull includes a point of the form $\{(0, y)\}$, where 0 is the origin, then set the maximum and minimum y -values at the origin as $y_{l,k1}$ and $y_{l,k0}$, respectively. Note that the convex hull calculated here includes points outside the embeddings. In practice, we do not need to compute the whole convex hull. Rather, we only need to solve a linear

programming problem. In the case of finding maximum values, given Euclidean embeddings $\{(x_{km}, y_{km})\}_{m=1}^{n_k}$, the problem is written as follows:

$$\begin{aligned} \max_{\{\lambda_m\}_{m=1}^{n_k}} \quad & \sum_{m=1}^{n_k} \lambda_m y_{km}, \\ \text{s.t.} \quad & \sum_{m=1}^{n_k} \lambda_m = 1, \\ & 1 \geq \lambda_m \geq 0. \end{aligned} \tag{50}$$

Then let the maximum of all $\{y_{l,k1}\}$ and the minimum of all $\{y_{l,k0}\}$ be y'_{l1} and y'_{l0} , respectively, and make them replacements for y_{l1} and y_{l0} .

Note that y'_{l1} (resp. y'_{l0}) is a valid lower (resp. upper) bound for y_{l1} (resp. y_{l0}), since there always exists a cone path geodesic between points in S_{l-1} that crosses $(0, y'_{l1})$ and $(0, y'_{l0})$. Also, as we can see from the proof of Theorem 10, this procedure assures that all geodesics between points in H_{l-1} that are not cone paths are always included in H_l .

References

- Bačák, M. (2013), ‘The proximal point algorithm in metric spaces’, *Israel Journal of Mathematics* **194**, 689–701.
- Bačák, M. (2014), *Convex analysis and optimization in Hadamard spaces*, Walter de Gruyter GmbH & Co KG.
- Benner, P., Bačák, M. and Bourguignon, P. Y. (2014), ‘Point estimates in phylogenetic reconstructions’, *Bioinformatics* **30**, i534–i540.
- Billera, L. J., Holmes, S. P. and Vogtmann, K. (2001), ‘Geometry of the space of phylogenetic trees’, *Advances in Applied Mathematics* **27**, 733–767.
- Bryant, D. (2003), ‘A classification of consensus methods for phylogenetics’, *DIMACS series in discrete mathematics and theoretical computer science* **61**, 163–184.
- Cule, M., Samworth, R. and Stewart, M. (2010), ‘Maximum likelihood estimation of a multidimensional log-concave density’, *Journal of the Royal Statistical Society. Series B: Statistical Methodology* **72**, 545–607.

- Degnan, J. H. and Salter, L. A. (2005), ‘Gene Tree Distributions Under the Coalescent Process’, *Evolution* **59**, 24.
- Felsenstein, J. (1978), ‘The Number of Evolutionary Trees’, *Systematic Zoology* **27**, 27–33.
- Felsenstein, J. (2004), *Inferring phylogenies*, Vol. 2, Sinauer associates Sunderland, MA.
- Kingman, J. F. C. (1982), ‘The coalescent’, *Stochastic Processes and their Applications* **13**, 235–248.
- Lubiw, A., Maftuleac, D. and Owen, M. (2020), ‘Shortest paths and convex hulls in 2D complexes with non-positive curvature’, *Computational Geometry: Theory and Applications* **89**, 1–42.
- MacQueen, J. and Others (1967), Some methods for classification and analysis of multivariate observations, in ‘Proceedings of the fifth Berkeley symposium on mathematical statistics and probability’, Vol. 1, Oakland, CA, USA, pp. 281–297.
- Nye, T. M. (2011), ‘Principal components analysis in the space of phylogenetic trees’, *Annals of Statistics* **39**, 2716–2739.
- Nye, T. M. W., White, . M. C. and White, M. C. (2014), ‘Diffusion on Some Simple Stratified Spaces’, *J Math Imaging Vis* **50**, 115–125.
- Owen, M. and Provan, J. S. (2011), ‘A fast algorithm for computing geodesic distances in tree space’, *IEEE/ACM Transactions on Computational Biology and Bioinformatics* **8**, 2–13.
- Pamilo, P. and Nei, M. (1988), ‘Relationships between gene trees and species trees.’, *Molecular Biology and Evolution* **5**, 568–583.
- Rannala, B. and Yang, Z. (2003), ‘Bayes estimation of species divergence times and ancestral population sizes using DNA sequences from multiple loci’, *Genetics* **164**, 1645–1656.
- Reid, N. M., Hird, S. M., Brown, J. M., Pelletier, T. A., McVay, J. D., Satler, J. D. and Carstens, B. C. (2014), ‘Poor fit to the multispecies coalescent is widely detectable in empirical data’, *Systematic Biology* **63**, 322–333.

- Rockafellar, R. T. (1970), *Convex analysis*, Princeton university press.
- Takahata, N. and Nei, M. (1985), ‘Gene genealogy and variance of interpopulational nucleotide differences’, *Genetics* **110**, 325–344.
- Vassilvitskii, S. and Arthur, D. (2006), k-means++: The advantages of careful seeding, in ‘Proceedings of the eighteenth annual ACM-SIAM symposium on Discrete algorithms’, pp. 1027–1035.
- Weyenberg, G., Huggins, P. M., Schardl, C. L., Howe, D. K. and Yoshida, R. (2014), ‘kdetrees: non-parametric estimation of phylogenetic tree distributions’, *Bioinformatics* **30**, 2280–2287.
- Weyenberg, G., Yoshida, R. and Howe, D. (2017), ‘Normalizing Kernels in the Billera-Holmes-Vogtmann Treespace’, *IEEE/ACM Transactions on Computational Biology and Bioinformatics* **14**, 1359–1365.
- Willis, A. (2019), ‘Confidence Sets for Phylogenetic Trees’, *Journal of the American Statistical Association* **114**, 235–244.
- Wu, Y. (2012), ‘Coalescent-based species tree inference from gene tree topologies under incomplete lineage sorting by maximum likelihood’, *Evolution* **66**, 763–775.